

Defibrillation of the heart: insights into mechanisms from modelling studies

Natalia Trayanova

Exp Physiol 2006;91;323-337; originally published online Feb 9, 2006;

DOI: 10.1113/expphysiol.2005.030973

This information is current as of December 18, 2007

This is the final published version of this article; it is available at:

<http://ep.physoc.org/cgi/content/full/91/2/323>

This version of the article may not be posted on a public access website for 12 months after publication, unless the article is open access.

Experimental Physiology is a publication of The Physiological Society. It has been published continuously since 1908. To subscribe to *Experimental Physiology* go to <http://ep.physoc.org/subscriptions>. *Experimental Physiology* articles are free 12 months after publication. No part of this article may be reproduced without the permission of Blackwell Publishing:
JournalsRights@oxon.blackwellpublishing.com

Defibrillation of the heart: insights into mechanisms from modelling studies

Natalia Trayanova

Department of Biomedical Engineering, Tulane University, New Orleans, USA

Despite its critical role in restoring cardiac rhythm and thus in saving human life, cardiac defibrillation remains poorly understood. Further mechanistic inquiry is hampered by the inability of presently available experimental techniques to resolve, with sufficient accuracy, electrical behaviour confined to the depth of the ventricles. The objective of this review article is to demonstrate that realistic 3-D simulations of the ventricular defibrillation process in close conjunction with experimental observations are capable of bringing a new level of understanding of the electrical events that ensue from the interaction between fibrillating myocardium and applied shock. The article does this by reviewing the results of two studies, one on vulnerability to electric shocks and another on defibrillation. An overview of the modelling tools used in these studies is also provided.

(Received 25 September 2005; accepted after revision 22 December 2005; first published online 9 February 2006)

Corresponding author N. Trayanova: Department of Biomedical Engineering, 500 Lindy Boggs Center, Suite 500, Tulane University, New Orleans, LA 70118, USA. Email: nataliat@tulane.edu (alternative Email: nataliat@cox.net)

Defibrillation of the heart by timely application of a strong electric shock is now recognized as the only effective means for prevention of sudden cardiac death. Despite the critical role that defibrillation therapy plays in saving human life, understanding of the mechanisms by which electric shocks halt life-threatening arrhythmias remains incomplete. Consequently, advancements in defibrillation procedure continue to be made largely by trial and error. While recent developments in experimental methodology have provided new characterizations of tissue responses to shocks, mechanistic inquiry into the success and failure of defibrillation is hampered by the inability of presently available experimental techniques to resolve, with sufficient accuracy, electrical behaviour confined to the depth of the ventricles during and after the shock. The objective of this review article is to demonstrate that realistic 3-D simulations of the ventricular defibrillation process in close conjunction with experimental observations are capable of bringing a new level of understanding of the electrical events that ensue from the interaction between fibrillating myocardium and applied shock, a level of understanding that is not possible to achieve by experiment alone. The article also provides an overview of the modelling tools used in attaining this goal.

Recent developments in the understanding of defibrillation mechanisms

Arrhythmia induction and defibrillation. The mechanisms of cardiac defibrillation have been strongly linked to cardiac vulnerability to electric shocks. A large body of research has demonstrated that an electric shock can induce ventricular arrhythmias if it is given during the ‘vulnerable window’ within the normal cardiac cycle (Wiggers, 1930). Furthermore, shocks that result in induction of arrhythmia are bound by a minimum and a maximum strength, termed the lower and upper limits of vulnerability (LLV and ULV; Fabiato *et al.* 1967). Fabiato *et al.* (1967) were the first to suggest that the mechanisms of induction and termination of ventricular fibrillation (VF) may be similar. This suggestion is now supported by the correlation between ULV and defibrillation threshold (DFT; Chen *et al.* 1986). For a defibrillation shock to succeed, it must extinguish existing VF activations throughout the myocardium (or in a critical mass of it), as well as not initiate new fibrillatory wavefronts. Extinguishing existing VF activations is not sufficient; the shock may still reinitiate VF by the same mechanism as it induces VF if applied during the vulnerable window. Therefore, understanding cardiac

vulnerability to electric shocks is a route to understanding defibrillation and arrhythmogenesis by failed shocks. In this light, the present article reviews both defibrillation and vulnerability studies. Finally, this article follows in the footsteps of numerous electrical and optical mapping studies of VF induction and defibrillation; it focuses on the mechanisms that govern the responses to the shock in the normal isolated heart preparation as a necessary step in solving the riddles of clinical defibrillation in diseased hearts.

Recent findings: virtual electrode polarization and the resulting post-shock behaviour. Over a decade ago, bidomain simulations (Sepulveda *et al.* 1989) followed by optical mapping studies (Knisley *et al.* 1994; Wikswa *et al.* 1995) demonstrated that the membrane response in the vicinity of a strong unipolar stimulus involved simultaneous occurrence of positive (depolarizing) and negative (hyperpolarizing) effects in close proximity. This finding of ‘virtual electrodes’ was in stark contrast with the established view that tissue responses should only be depolarizing (hyperpolarizing) if the stimulus was cathodal (anodal) (Hodgkin & Rushton, 1946). Since then, virtual electrode polarization (VEP) has been documented in experiments and simulations involving field stimulation with various electrode configurations (Efimov *et al.* 1998, 2000c; Knisley *et al.* 1999). Detailed analysis of VEP aetiology demonstrated that both applied field (Sobie *et al.* 1997; Knisley *et al.* 1999) and tissue structure (Trayanova & Skouibine, 1998; Knisley *et al.* 1999; Trayanova, 2001) are major determinants of the shape, location, polarity and intensity of the shock-induced polarization (Trayanova *et al.* 1998b; Trayanova, 1999; Hooks *et al.* 2002; Rodriguez & Trayanova, 2003; Rodriguez *et al.* 2005).

The cellular response to shock-induced VEP depends on the strength and polarity of the shock, as well as on the electrophysiological state of the cell at the time of shock delivery. Positive VEP can result in regenerative depolarization in regions where tissue is at or near diastole; such activation is termed ‘make’ because it takes place at the onset (make) of the shock. Furthermore, action potential duration can be either extended (by positive VEP) or shortened (by negative VEP) to a degree that depends on VEP magnitude and shock timing (Efimov *et al.* 2000b). Finally, strong negative VEP can completely abolish (de-excite) the action potential (i.e. regenerative repolarization), thus creating post-shock excitable gaps in the virtual anode regions. The close proximity of a de-excited region and a virtual cathode has been shown, in both modelling studies (Roth, 1995) and optical mapping experiments (Wikswa *et al.* 1995), to result in an excitation at shock end (termed ‘break’ excitation, i.e. at the break of the shock). The virtual cathode serves as an electrical stimulus eliciting a regenerative depolarization and a propagating wave in the newly created excitable gap.

Break activations arise at the borders between oppositely polarized regions provided that the transmembrane potential gradient across the border spans the threshold for regenerative depolarization (Cheng *et al.* 1999a). A shock succeeds in extinguishing fibrillatory wavefronts and not initiating new re-entry if make/break excitations manage to traverse the shock-induced excitable gaps before the rest of the myocardium recovers from shock-induced depolarization (Efimov *et al.* 2000b; Skouibine *et al.* 2000a; Rodriguez *et al.* 2005). Thus, latency in the onset of these excitations, their propagation velocity through the excitable gaps, and shock-induced extension of refractoriness in the depolarized areas determine how quickly post-shock activity subsides following successful shocks (Cheng *et al.* 1999a; Skouibine *et al.* 2000a; Trayanova *et al.* 2002b).

Vulnerability to electric shocks and defibrillation failure can also stem from the shock-induced VEP. Make excitation can result in the formation of a new re-entry via the critical point mechanism (Winfrey, 1987), where a phase singularity is formed at the intersection of a critical level of shock-induced depolarization and a critical level of recovery of a preshock wave. The onset of a break excitation is also associated with the formation of a (VEP-induced) phase singularity (Efimov *et al.* 1998); it forms at a point along the boundary between shock-induced depolarization and de-excitation (Efimov *et al.* 2000c) and is independent of the preshock state of the myocardium. If these phase singularities survive, allowing a spiraling wavefront to develop, the shock results in the (re)initiation of re-entrant arrhythmia.

The continued search for answers. The majority of the findings above were reported in isolated rabbit heart studies; activity in these experiments was mapped optically over an epicardial area typically limited to the vicinity of the electrodes. In studies by Knisley’s group (Knisley *et al.* 1994, 1999), a window of 6 × 6 mm was scanned; Kwaku & Dillon (1996) scanned 100 sites over 30% of the rabbit anterior epicardium. Publications by Efimov *et al.* (1998, 2000a,c) documented behaviour within a 16 × 16 mm window that occupied about half of the anterior epicardium of the rabbit ventricles over the right ventricle (RV) catheter; the observed break excitations originated at the border of regions of opposite-sign strong polarization that occurred above the shock electrode. Thus, the global effect of the shock, as well as the post-shock activity that ensued from it, could not be observed in these studies. Dual CCD camera simultaneous anterior and posterior recordings allowed Gray and coworkers (Evans *et al.* 2002; Trayanova *et al.* 2003) to map the effect of the shock over the majority of the epicardium in Langendorff-perfused rabbit heart preparations. Records of epicardial activity revealed that the aetiology of post-shock excitation is

more complex than previously believed. For instance, post-shock activations were shown to originate away from (Evans *et al.* 2002), rather than in the vicinity of (Efimov *et al.* 1998), the shock catheter. In the study by Evans *et al.* (2002), global epicardial activity following shocks of the same strength but reversed polarity was radically different from activity observed, under similar conditions, in the vicinity of the catheter (Efimov *et al.* 2000c). This indicates that anatomical features and geometrical asymmetries in the heart could significantly affect global post-shock propagation.

Mapping the entire epicardial surface of the ventricles, a course that most recent developments in optical mapping have taken, will not, however, reveal the global 3-D activity that follows the shock. Activations could propagate intramurally, without a signature on the epicardial surface (Winfree, 1988). While reports disagree on the depth of penetration of the optical signal, it is clear that the spatiotemporal characteristics of activity in the depths of the myocardium cannot presently be resolved; efforts to achieve this, although promising, remain at a nascent stage (Hooks *et al.* 2001; Byars *et al.* 2003). The problem is particularly aggravated in post-shock arrhythmogenesis, since there is a dramatic difference between the magnitude and pattern of shock-induced VEP in the surface layers and in the depth of the myocardium. As determined by simulation studies (Trayanova *et al.* 1998b; Entcheva *et al.* 1999), these differences emanate from the different mechanisms that govern surface polarization and polarization in the tissue bulk. Such differences in VEP could result in different electrophysiological behaviour on the surfaces and in the depth. Thus, it is feasible that midmyocardial post-shock activity could remain confined to the depth of the ventricular wall and detached from surface post-shock behaviour for significant stretches of time.

From this brief review, it is apparent that, despite numerous advancements in understanding the mechanisms of shock-induced arrhythmogenesis and defibrillation, the global 3-D post-shock behaviour in the ventricles remains largely unknown. Contributions of ventricular anatomical features to VEP and post-shock propagation patterns have never been quantified. Most importantly, the characteristics of post-shock electrical activity in the depth of the myocardium cannot be presently be resolved. Below we present recent results from our laboratory demonstrating how these questions can be answered using a realistic computer model of defibrillation in close conjunction with experimental studies.

Multiscale modelling of defibrillation

This section provides an overview of the modelling tools used in our recent studies of defibrillation. Over the last

several years, our laboratory has developed a 3-D finite-element bidomain model of the rabbit ventricles for use in defibrillation studies. The model has been described in detail in our recent publications (Trayanova *et al.* 2002a, 2004; Trayanova & Eason, 2002; Aguel *et al.* 2003; Rodriguez *et al.* 2005). Here we briefly outline its major components.

Description of myocardial geometry and fibre architecture. Our 3-D model of anatomically based rabbit ventricular geometry and fibre orientation used the University of California San Diego geometrical model of the rabbit ventricles (Vetter & McCulloch, 1998). The original geometry was defined in prolate spheroidal coordinates which we translated into Cartesian coordinates. We used MSC Patran (MSC Software Corporation, Santa Ana, CA, USA) to generate the computational grids. The surfaces and the 'solids' of the mesh were created with Patran functions. Additional 'solids' were generated to represent the ventricular cavities and the perfusing bath; the conductivity of these regions was assigned the value of blood. Using Patran, surfaces and solids were meshed to create unstructured triangular and tetrahedral meshes, respectively, with an average element edge length of 300–500 μm in the tissue and 1 mm in the cavities and the perfusing bath. Once the entire mesh was complete, files containing node coordinates, elemental connectivity, and the original finite element to which each tetrahedral element in the new mesh belongs were generated. This information was then used to determine, with the combination of two multidimensional root-finding algorithms, fibre orientation at the centroid of each tetrahedron. Local material properties were assigned to each element using the fibre orientations. Figure 1 illustrates the 3-D geometry and fibre orientation in the rabbit ventricles as determined by this algorithm.

Tissue representation. In simulation studies of defibrillation, mathematical description of cardiac tissue is based on the bidomain representation, which considers the tissue to be composed of intra- and extracellular spaces separated by a membrane. In the rabbit ventricular model, the myocardium was characterized with unequal anisotropy ratios in the intra- and extracellular conductivities. The potentials in the ventricular cavities and the perfusing bath were governed by the Laplace equation; conductivities in these domains were assigned the value of blood.

Numerical solutions for the bidomain equations employed the semi-implicit finite element method (Eason & Trayanova, 2002; Aguel *et al.* 2003; Rodriguez *et al.* 2005).

Representation of ionic currents and membrane electroporation. Our group has assembled a library of membrane models, including versions of Beeler-Reuter

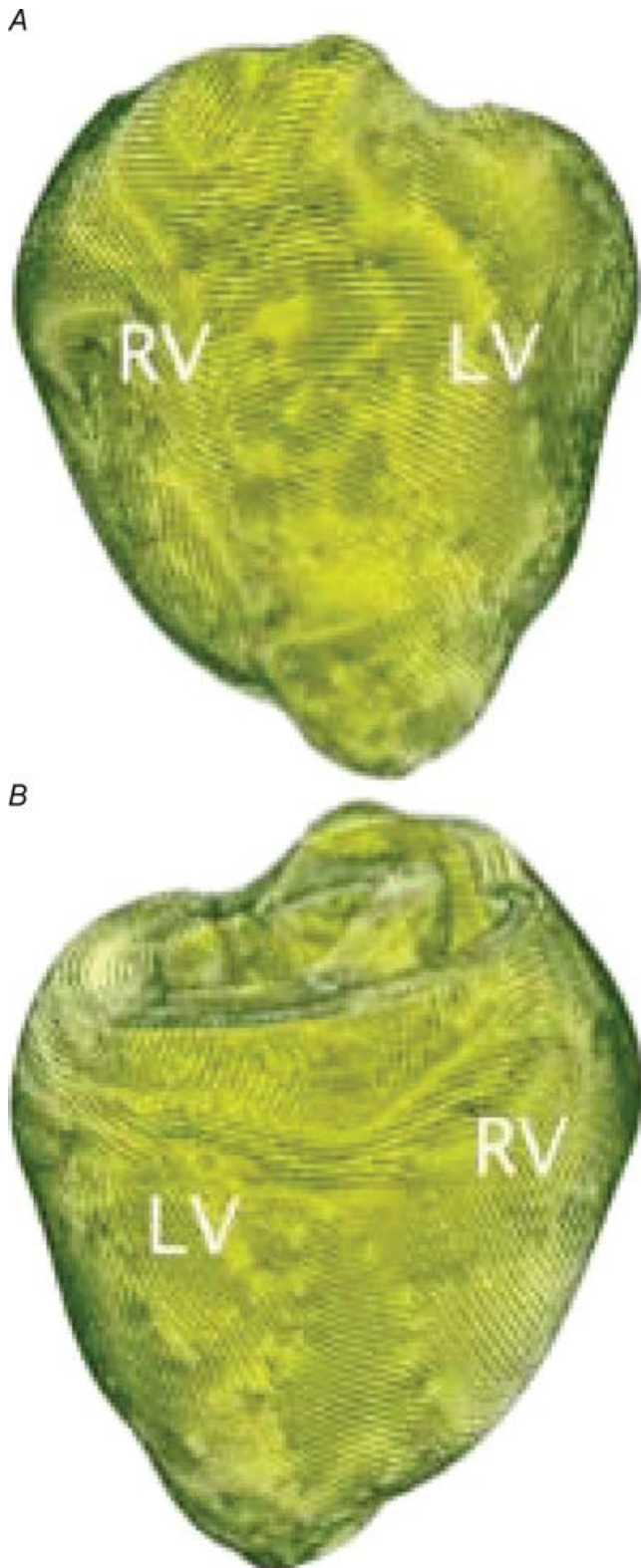


Figure 1. Rabbit ventricular geometry and fibre orientation (shown by tiny lines)

A, posterior view; *B*, anterior view.

(BR; Beeler & Reuter, 1977) and Luo Rudy (LR1 and LRd) models and their recent modifications (Luo & Rudy, 1991, 1994; Faber & Rudy, 2000), all of which have been employed in some aspect of our computational electrophysiology research. Figure 2 shows fibrillation in the rabbit ventricular model induced by a train of 12 rapid pacing stimuli; the membrane model is LR1 with steep restitution properties. For defibrillation studies, all membrane models were further modified to ensure stability during the shock (Skouibine *et al.* 2000*b*) when a dramatic change in transmembrane potential takes place. It is important to understand, however, that defibrillation shocks induce complex changes in transmembrane potential, some of which have been consistently observed in experiments but never reproduced by membrane models, mostly because membrane models were developed for the study of action potential conduction and arrhythmogenesis and not defibrillation. These observed phenomena are as follows. First, strong shocks applied during action potential plateau in isolated guinea-pig papillary muscle (Zhou *et al.* 1995), cultured neonatal rat myocyte strands (Fast *et al.* 2000), and isolated guinea-pig myocytes (Cheng *et al.* 1999*b*) induce asymmetrical changes in transmembrane potential (V_m) with the negative transmembrane potential change (ΔV_m^-) being larger than the positive change, i.e. $\Delta V_m^- > \Delta V_m^+$. Second, with increase in shock strength, ΔV_m magnitude does not increase proportionally but instead saturates (Zhou *et al.* 1995; Fast *et al.* 2000). Third, for large shock strengths, ΔV_m^- exhibits non-monotonic behaviour with an initial rapid increase and then a decrease (Cheng *et al.* 1999*b*; Fast *et al.* 2000). None of the present membrane models reproduces these responses to strong shocks. Since the purpose of creating the rabbit ventricular model of defibrillation is to unravel the mechanisms of post-shock behaviour observed experimentally, we

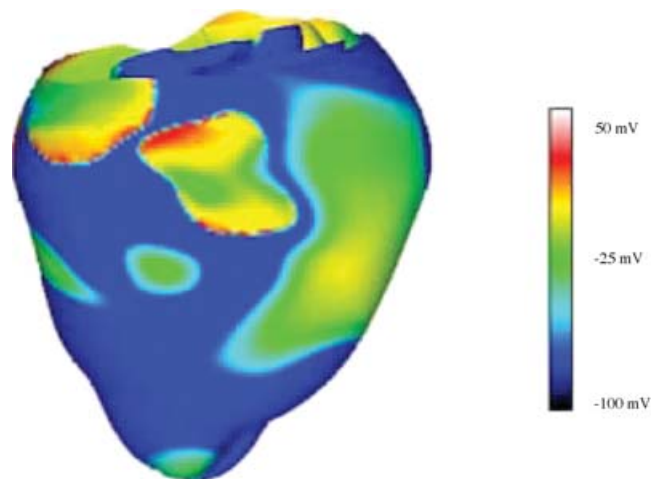


Figure 2. Anterior transmembrane potential distribution in a model of the fibrillating rabbit ventricles

needed first to make sure that the membrane model we use reproduced the behaviour described above. This necessitated membrane model modifications.

Using a recent version of the *LRd model* (Faber & Rudy, 2000), we found that the negative bias in ΔV_m asymmetry could not be reproduced by the natural addition of electroporation (*model LRd + EP*), the latter documented always to take place following strong shocks (Al Khadra *et al.* 2000). Only when we incorporated the outward current activated upon strong shock-induced depolarization (I_a), first suggested by Cheng *et al.* (1999b), did we achieve a match between simulation and experiment (Fig. 3), provided we assumed that I_a was part of the K^+ flow through the L-type Ca^{2+} channel (the model was termed *aLRd model*). With the use of the new *aLRd model* we were able to reproduce the experimentally observed rectangularly shaped positive V_m transient: negative-to-positive V_m ratio of near 2 (Cheek *et al.* 2000; Fast *et al.* 2000); stronger electroporation at the anode (Cheek & Fast, 2004); and dependence of ΔV_m

magnitude on field strength (compare Fig. 3 to Cheek *et al.* 2000; Fast *et al.* 2000). Being equipped with a membrane model, such as the *aLRd*, that can accurately reproduce the membrane responses to shocks (Ashihara & Trayanova, 2004) was essential to our ability to simulate tissue and organ behaviour observed experimentally, and thus to provide insight about behaviour in the depth of the tissue that cannot be assessed by the presently available experimental techniques.

Shock electrodes and waveforms. In the rabbit model, shock electrodes were represented as 3-D iso-current density or iso-voltage surfaces within the 3-D computational grid (ventricles plus perfusing bath and blood in cavities); these were chosen to mimic geometry and location of electrodes in optical mapping experiments. The examples in this article include external plate (at the boundaries of the perfusing chamber) and cuff electrodes (Fig. 4); we have also implemented an RV catheter and a return electrode in the posterior bath (not

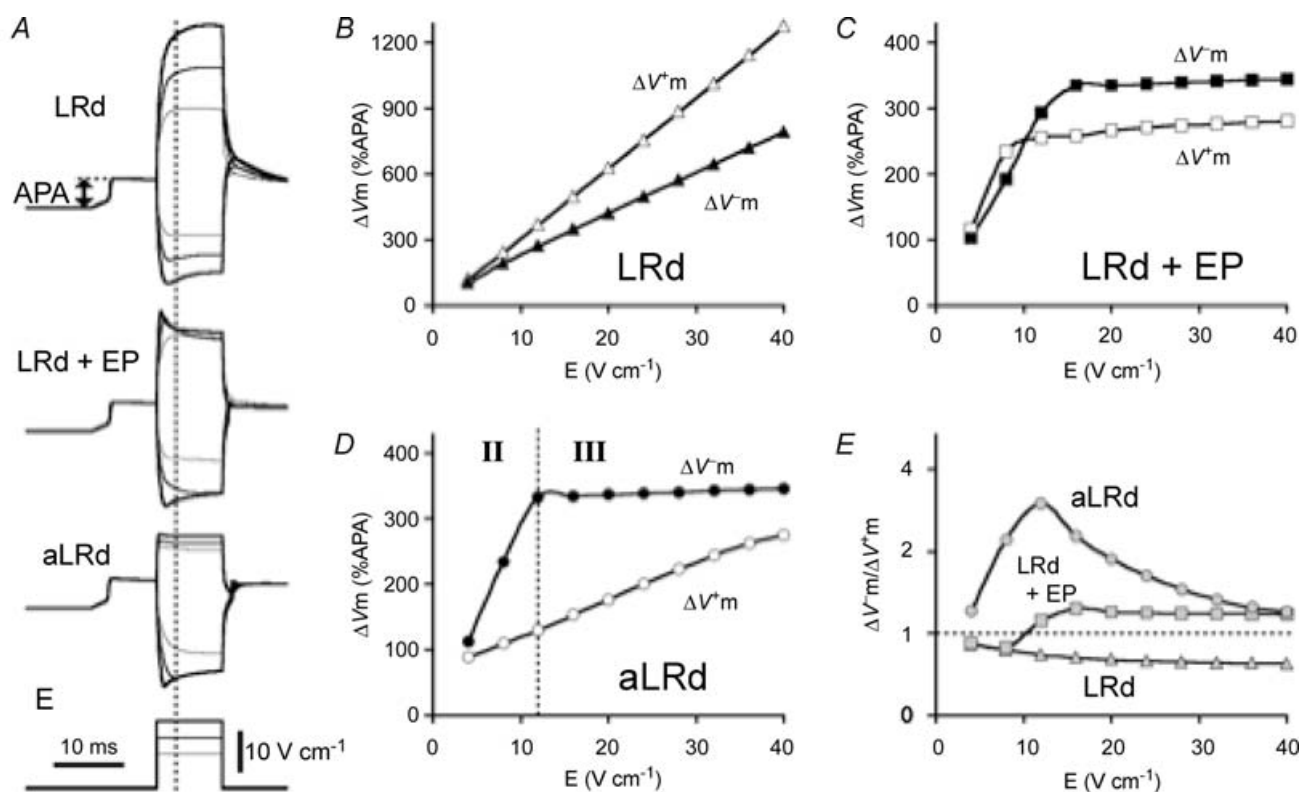


Figure 3. Responses to shocks of various strengths (E) delivered during the plateau ($CI = 10$ ms) in a $800 \mu\text{m}$ long fibre

A, superposition of shock-induced VEP at the fibre ends. Membrane kinetics are represented by the LRd, LRd with electroporation (LRd + EP), and augmented LRd (aLRd) models. Shock duration is 10 ms and strengths are 8, 12 and 16 V cm^{-1} (thin, thicker and thickest continuous lines, respectively). APA is action potential amplitude. Vertical dotted line indicates time of ΔV_m measurement, 3 ms after shock onset. B, C and D, shock-induced positive and negative ΔV_m as a function of shock strength for the three models. Characters II and III denote types of non-linear responses, as per Fast *et al.* (2000). E, $\Delta V_m^-/\Delta V_m^+$ ratio as function of shock strength in the three models. Reproduced with permission from Ashihara & Trayanova (2004).

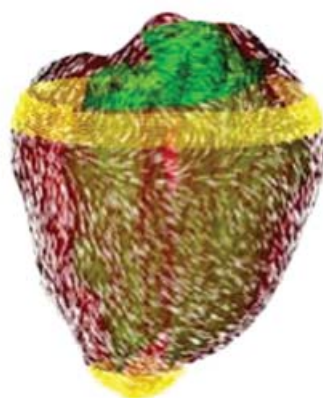
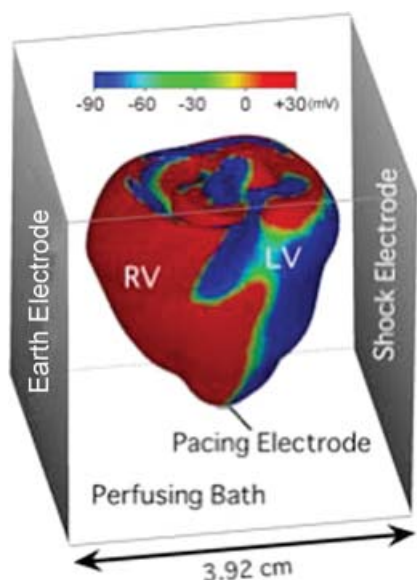


Figure 4. Defibrillation electrode configurations used in the examples presented in this article

Left panel, external large plate electrodes, which provide a uniform applied field. The size of the perfusing chamber is indicated in the figure, as well as the location of the pacing electrode at the apex. The heart is experiencing virtual electrode polarization by the defibrillation shock. Right panel, cuff electrodes shown over the ventricular surfaces and epicardial fibre orientation.

shown here). The waveforms used in our vulnerability and defibrillation studies include (truncated exponential) mono- and biphasic shocks (Trayanova & Bray, 1997; Anderson *et al.* 2000; Anderson & Trayanova, 2001; Rodriguez *et al.* 2004a,b, 2005).

Scroll-wave filament postprocessing. To permit better analysis of the post-shock behaviour in the rabbit ventricles, we developed postprocessing that allows us to investigate the dynamics of scroll-wave filaments, the organizing centres of re-entrant activity (Eason &

Trayanova, 2002; Trayanova & Eason, 2002; Ashihara *et al.* 2004; Trayanova *et al.* 2004). We quantify the number of filaments, the length of each filament, its lifespan and its location in the left and right ventricular (LV and RV) free wall, or septum. In addition, we document the type of each filament: I, U or O. Type I is assigned to a filament the ends of which are in contact with the endo- and epicardial surfaces of the LV or RV free walls, or the endocardial surfaces of the LV and RV in the case of a septal location. Type U is a filament both ends of which are in contact with an endo- or epicardial surface. A filament of type O is a closed loop (vortex ring). An example of each type of filament is shown in Fig. 5. In addition, filaments of transitional type that do not fit the classification are also identified. Elucidating post-shock filament behaviour is an important component in the quest for clarifying the defibrillation mechanisms.

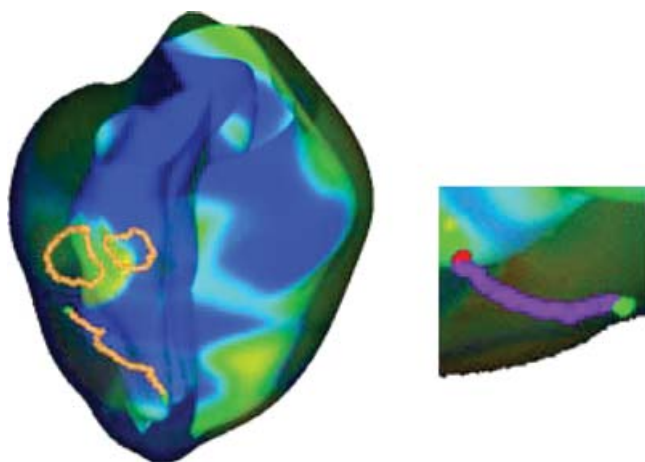


Figure 5. Scroll-wave filaments in the rabbit ventricles

Left panel, two type O filaments and a long type U filament in a semi-transparent rendering of the rabbit ventricles undergoing fibrillation. Filaments are shown in orange. Endings of the type U filament are coloured in green, an indication that they are in contact with the endocardial surface. Right panel, a cut-out from the rabbit LV illustrating type I filament. The filament is shown in purple, and its ends are coloured in green and red, indicating contact with the endo- and epicardial surfaces, respectively.

Role of 3-D ventricular anatomy in vulnerability and defibrillation

In this section, we present two studies, one on cardiac vulnerability to electric shocks (Rodriguez *et al.* 2005) and another on defibrillation (Trayanova *et al.* 2004), that illustrate the capabilities of the model and address questions raised in the beginning of this article regarding the role of ventricular anatomy in these processes.

Arrhythmogenesis following shocks administered to an isolated, paced rabbit heart. The goal of this study was to investigate the role of ventricular anatomy, specifically the geometrical differences between LV and RV in vulnerability to electric shocks. Since spatial non-uniformity of the applied electric field has been implicated in generating shock-induced polarization in addition to

polarization stemming from tissue geometry and fibrous structure (Trayanova *et al.* 1998a; Trayanova & Skouibine, 1998; Skouibine *et al.* 1999; Trayanova, 1999; Lindblom *et al.* 2000, 2001) and is therefore a factor in shock outcome, a uniform applied field (as delivered by large external plate electrodes) was used. In this case, reversal of shock polarity acts only to change the direction of the current flow through the ventricular chambers. This allowed us to examine, for the same magnitude and configuration of the applied field, how differences between LV and RV chamber anatomy result in differences in shock-induced transmembrane potential changes and post-shock electrical activity, and thus in shock outcome. Of particular importance is knowledge regarding the location of the main post-shock excitable area formed typically by de-excitation of previously refractory myocardium (Efimov *et al.* 2000a; Trayanova *et al.* 2002a; Hillebrenner *et al.* 2003, 2004) in a large portion of the ventricular volume. Post-shock wavefront propagation through it is characterized by long uninterrupted pathways (Trayanova *et al.* 1999; Rodriguez & Trayanova, 2003) allowing for the recovery of the surrounding myocardium. Therefore, the main post-shock excitable area is directly responsible for the global electrical behaviour of the ventricles following the shock and ultimately, for shock outcome. To permit full elucidation of the role of ventricular anatomy in shock-induced vulnerability, this study used a combination of optical mapping experiments and 3-D computer simulations.

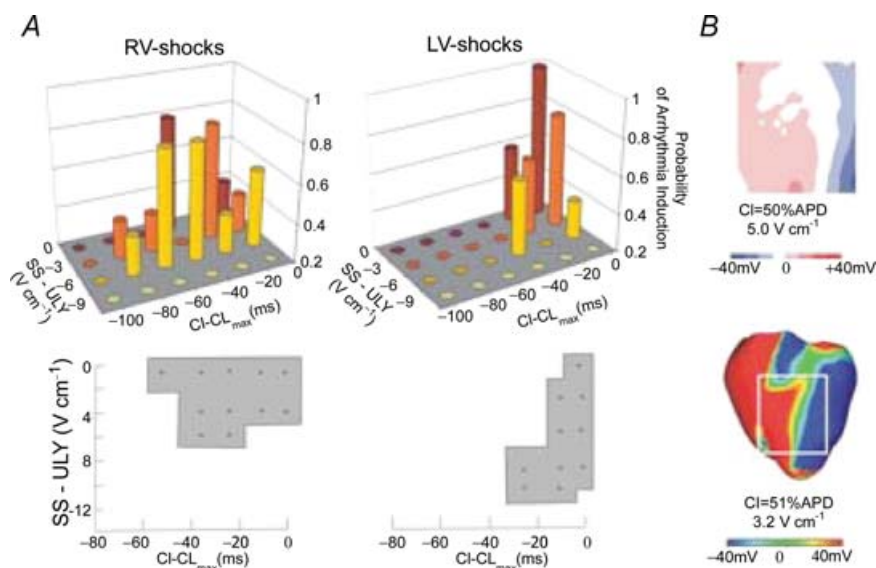
In simulations and experiments, the ventricles were paced at the apex. To ensure uniform applied field, in both approaches the shocks were delivered via two large planar electrodes located at the vertical walls of the perfusion chamber (Fig. 4, left panel). Consistent with the goal of the study, examining the change in cardiac vulnerability

upon reversal of field direction necessitated the use of monophasic shocks in both simulations and experiments (8 ms duration truncated exponential waveforms of 65% tilt). The shocks were applied over a range of coupling intervals (CIs, measured with respect to the last pacing stimulus). The applied electric field was referred to as RV when the electrode near the RV was used as the cathode and the one near the LV was the earth electrode. The opposite electrode orientation was referred to as LV. Shock strength (SS) referred to the leading edge value of the electric field between the electrodes. Vulnerability areas (VAs), i.e. areas on a 2-D grid that encompass episodes of re-entry induction for various SSs and CIs, were determined for both field directions in simulations and in experiments. For each field direction, the ULV was estimated as the highest shock strength that induced sustained arrhythmia. The vulnerable window was estimated to be the interval in time between the lowest and the highest CI at which a sustained arrhythmia was induced.

Figure 6A demonstrates that the probability of arrhythmia induction is distributed differently over SSs and CIs for the two field directions. In order to combine data from different experiments, SS and CI were represented as deviations from the ULV and the longest CI in the vulnerable window (CI_{max}), respectively. In the experiment (Fig. 6A, top panel), for RV shocks, a probability of arrhythmia induction greater than 0.2 (i.e. occurring in at least 2 rabbits) was documented for a wide range of CIs ($CI - CI_{max}$ from 0 to 80 ms) and for SSs ranging from 0 to 6 $V\ cm^{-1}$ SS-ULV. For LV shocks, a probability of arrhythmia induction larger than 0.2 was found to concentrate within a much narrower CI range ($CI - CI_{max}$ from 0 to 40 ms). In addition, in all hearts examined, ULV occurred at CI_{max} for LV shocks, and over a range of CIs for RV shocks (mean ULV values

Figure 6. Shocks of reversed Polarity

A, vulnerability areas (VAs) for RV and LV shocks in experiment (top) and simulation (bottom). In the top panel, vertical axes represent probability of arrhythmia induction in 5 experiments. In the bottom panel, dark areas represent VAs, and asterisks denote episodes of shock delivery. Shock strength (SS) and coupling interval (CI) are calculated as deflections from ULV and CI_{max} . B, optical map of shock-end potentials from 1 rabbit and the corresponding simulated potential distribution. The white box in the simulation panel outlines the location of the optical field of view in the experiment. The figure is a combination of parts of figures from Rodriguez *et al.* (2005), reproduced with permission.



in the experiment were 12.2 ± 1.6 and 11 ± 2.1 V cm⁻¹ for RV and LV shocks, respectively). The bottom panel of Fig. 6A presents VAs for both field directions as obtained from the rabbit ventricular model. For RV shocks (ULV = 9.6 V cm⁻¹), consistent with the experimental data, VA extends over a broad CI range, from 0 to 60 ms CI–CI_{max} and for SS ranging from 0 to 6.4 V cm⁻¹ SS–ULV. In addition, as in the experiment, it has a somewhat rectangular shape. Reversing field direction (ULV = 12.7 V cm⁻¹) alters VA shape in a manner similar to experimental data: the majority of arrhythmias are induced at long CIs, from 0 to 20 ms CI–CI_{max}, and ULV is reached at CI_{max}. Furthermore, in simulations as in experiments, only shocks of strength less than 8 V cm⁻¹ induce arrhythmia when applied at short CIs (CI–CI_{max} less than 20 ms).

The correspondence between experimental and model VAs is qualitatively very good, as demonstrated by Fig. 6A. Similarly impressive is the match between simulation and experiment regarding the epicardial VEP (Fig. 6B): for RV shocks, in both experiments and simulations, the epicardium is depolarized in the vicinity of the cathode, while the LV epicardium is negatively polarized; reversing field direction switches, overall, the location of these two areas. To elucidate the mechanisms underlying the change

in vulnerability upon reversal of the direction of applied field, however, one needs to rely on insight obtained solely through realistic simulations of 3-D electrical activity.

The difference in the 3-D shock-end transmembrane distributions between the two cases is examined in Fig. 7 for episodes inside and outside the VA. For RV shocks (Fig. 7, left panel), one observes that increasing SS by 6.4 V cm⁻¹ from below to above the ULV for the same CI, i.e. moving vertically across the VA border (compare episode *b* to episode *a*), results in an increase in the areas strongly depolarized by the shock; the trend remains the same when CI is increased (compare episodes *c* and *d*). Furthermore, the simulation results in the left panel of Fig. 7 demonstrate that for this orientation of the applied field, regardless of SS or CI, the main post-shock excitable area is always within the LV wall (deep blue areas). The shock-end negative polarization in the RV is a thin stripe in a thin wall; the RV is thus not a major structure for post-shock propagation. For instance, in case *b*, by the time the wavefronts propagate through the LV excitable area, the rest of the myocardium recovers, allowing re-entry to be established. Two rotors are induced, one anticlockwise and one clockwise, on the anterior and posterior sides of the ventricles, respectively, with a common pathway in the apex (Fig. 8, top panel). The same re-entrant pattern

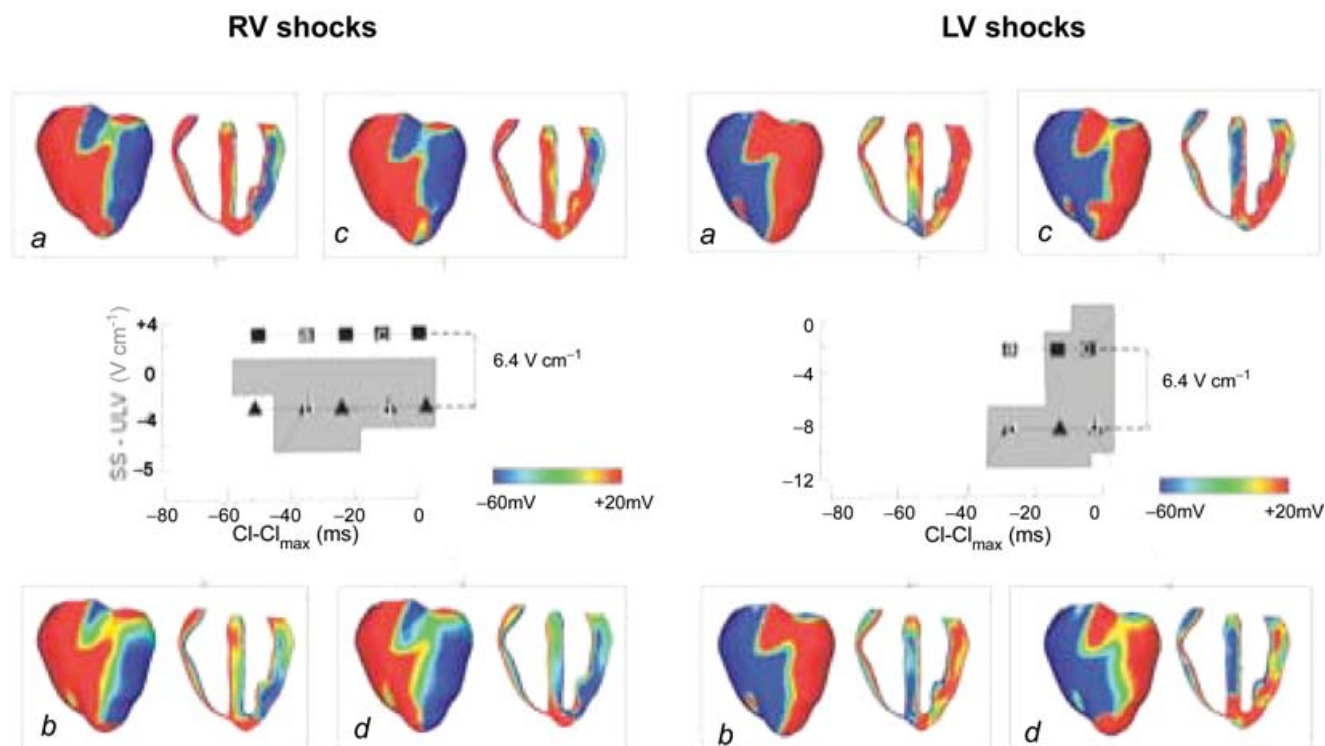


Figure 7. Simulated transmembrane potential distributions at shock-end on the anterior epicardium and in a transmural view of the rabbit ventricles for RV and LV shocks within and outside the vulnerable area

Reproduced with permission from Rodriguez *et al.* (2005).

was observed in the experiment as documented by the activation map shown in the top panel of Fig. 8. This behaviour is similar for every CI in the VA, hence the nearly rectangular shape of the VA for RV shocks.

The right panel of Fig. 7 presents analysis of the shock-end V_m distribution for LV shocks; here the effect of increased SS is different for short *versus* long CIs. First, for intermediate and long CIs (i.e. intermediate and small $CI - CI_{max}$), the 6.4 V cm^{-1} change in SS results in an episode within the VA. Second, for LV shocks the main post-shock excitable area relocates to the septum, the other thick wall in the ventricles (Fig. 7, right panel). For episodes within the VA, as shown in the bottom panel of Fig. 8, the septal excitable area results in the establishment of re-entry. The re-entrant circuit is a figure of eight on the anterior and another on the posterior with a common pathway in the LV, and is also evident in the experimental activation map in the bottom panel of Fig. 8. The pattern of the re-entry is indeed determined by the initial post-shock propagation, here through the septum, resulting in subsequent activation through both free walls. The septal excitable area is, however, minor and thus inconsequential in episode *a* shown in the right panel of Fig. 7, causing a no-arrhythmia induction outcome of episode *a* and thus altering the VA shape. Therefore, for LV shocks, the unusual behaviour of the septum for short CIs and large

SSs results in a VA shape that differs from the one for RV shocks.

The combination of optical mapping experiments and 3-D computer simulation studies creates, as demonstrated by the present study, a unique opportunity to explore cardiac electrical behaviour following a defibrillation shock. The simulations provide information regarding behaviour in the depth of the ventricular walls (including the septum) unachievable by any imaging technique thus far. This study revealed that ventricular anatomy plays a major role in shock-induced electrical behaviour, and thus in the outcome of a defibrillation shock. The difference in the thickness of the ventricular walls is ultimately manifested as a preferential location of the post-shock excitable area. In addition, the location of this area determines the types of post-shock re-entrant circuits. The findings of the study are directly applicable to external defibrillation with monophasic shocks. They are also very relevant to implantable cardioverter defibrillator (ICD) electrode configurations and biphasic waveforms. In these more complex cases, a main post-shock excitable area(s) will still be developed within the 3-D volume of the tissue; it will be at least partly determined by cardiac anatomy. Identifying the location of the main post-shock excitable area could be very important for improving clinical defibrillation efficacy, since its eradication can be

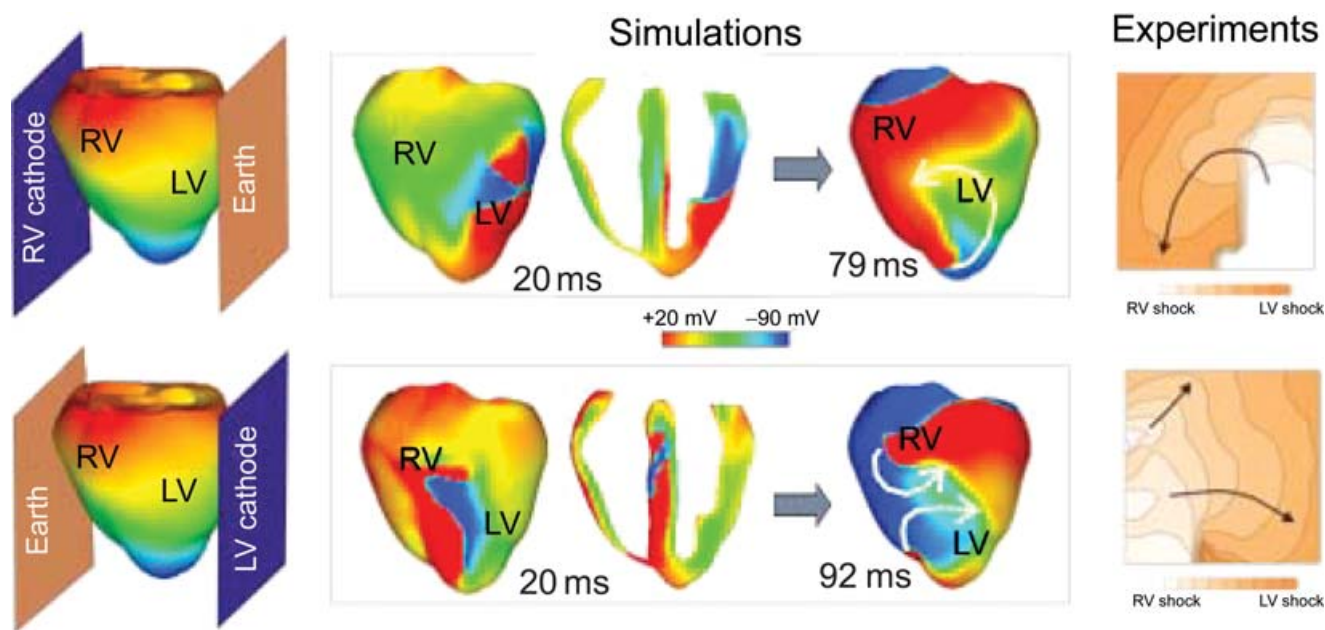


Figure 8. Evolution of post-shock activity for RV shocks (top panel), and LV shocks (bottom panel)

For the simulations, the episode in the top panel corresponds to episode *b* in Fig. 7, RV shocks, while the episode in the bottom panel is episode *b* from Fig. 7, LV shocks. Anterior epicardial and some transmural views of transmembrane potential distribution are shown. White arrows represent direction of propagation. Colour scale as in Fig. 7. The experiments show optical imaging activation maps on the anterior surface of a rabbit heart for RV and LV shocks within the vulnerable area. Black arrows indicate direction of propagation. In both simulations and experiments, RV shocks result in a single spiral wave, while LV shocks establish a figure-of-eight re-entry on the anterior epicardium. This figure is based on figures from Rodriguez *et al.* (2005).

specifically targeted by auxiliary small magnitude shocks, resulting in a dramatic decrease in defibrillation threshold.

Spatiotemporal organization of 3-D electrical activity following defibrillation. Understanding the complex spatiotemporal dynamics of post-shock activity in the heart could be aided by the tools of non-linear dynamics (Gray *et al.* 1998; Larson *et al.* 2003). Instead of the evolution of transmembrane potential distribution in the myocardium, these tools analyse the dynamics of the phase singularities, which represent the organizing centres of re-entrant activity. Applying this approach to the post-shock activity in the 3-D volume of the rabbit model ventricles allows examination of the evolution and behaviour of the transmural post-shock filaments, the 3-D strings of phase singularities. This avenue provides a new opportunity to clarify the interaction of the shock with the preshock phase singularities that underlie VF, to evaluate how the shock itself creates phase singularity filaments, and to

examine the behaviour of these filaments for failed and successful shocks. The present study provides insight into some of these issues. Specifically, it aims: (1) to establish a relationship between spatiotemporal post-shock filament dynamics, particularly the change in filament shape and location within the ventricles, and shock outcome; and (2) to relate the complexity of the preshock state (phase of VF) to shock efficacy.

Figure 9 presents three instances of post-shock activity following a successful defibrillation shock delivered to the fibrillating ventricles shown in Fig. 2. The shock was of strength 154.12 mA and was given at a shock timing of 1300 ms after VF initiation. This figure shows posterior and apical (from apex to base) semi-transparent views of both transmembrane potential and filament distributions. The 1310 ms panels depict the virtual electrode polarization at the end of the 9 ms shock and the high number of scroll-wave filaments induced by the shock. By 1320 ms, propagating wavefronts have begun

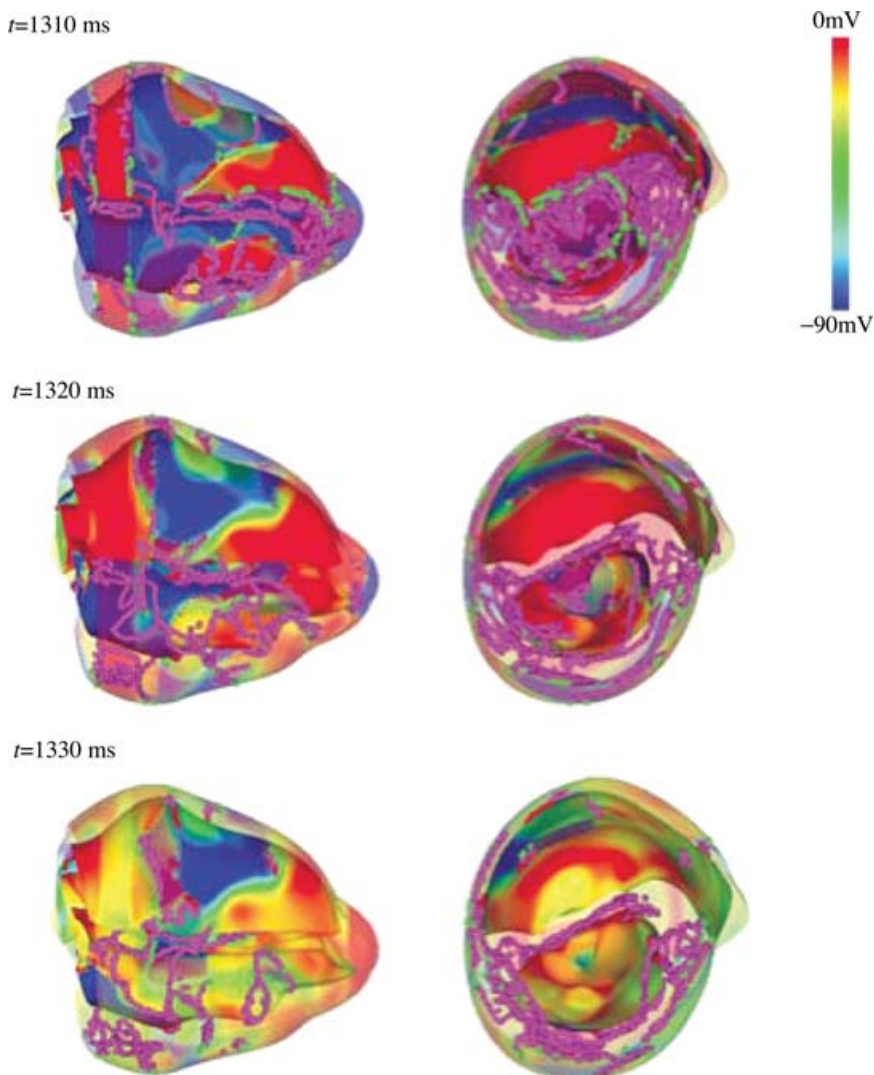


Figure 9. Posterior and apical (apex to base) semi-transparent views of the transmembrane potential with superimposed filament distribution (in purple)

Each set of panels portrays different times of post-shock activity. Time is counted since the end of the shock.

to invade de-excited tissue (blue areas), and the number of filaments present has decreased owing to filament annihilation and aggregation in the limited volume of the ventricles. By 1330 ms, the number of filaments has significantly decreased. All defibrillation episodes, both successful and failed, produced post-shock behaviour similar to the one portrayed in Fig. 9 over the same post-shock time interval.

The post-shock activity was quantified in Fig. 10, which presents the number of post-shock filaments as a function of the time after shock application. All defibrillation episodes are characterized by a large initial number of filaments. On average, successful shocks have a slightly larger number of filaments at 30 ms post-shock compared to failed shocks (19.8 *versus* 17.5 filaments). The number of filaments quickly decreases in the first 100 ms after the shock delivery, with a somewhat faster decrease in the 50 ms immediately following the shock. The only exception from this trend here is the weakest shock, 25.69 mA. At 30 ms after the shock, this shock strength results in only six filaments: four in the RV and two in the septum.

Figure 10 also demonstrates that in all cases, the interval of 100–250 ms following the shock is characterized by increased organization in ventricular electrical behaviour: the number of filaments is relatively small and nearly constant. For the four successful shocks spanning current densities from 106.35 to 128.43 mA, the number of post-shock filaments in the interval 100–200 ms is the smallest. In fact, there are only two filaments for each successful shock at 100 ms post-shock. The filaments associated with the successful shocks disappear completely within the interval of 200–250 ms following the shock. For

failed shocks (strengths 25.69–105.35 mA), the number of filaments remains larger in the interval 100–200 ms (it averages 5.25 at 100 ms) and begins to rise again at about the 200 ms mark, signifying the transition to a more disorganized behaviour.

Figure 11 examines the type of the filaments and their location in the ventricles. Three timings following the shock, 30, 100 and 300 ms, are presented for each location. The individual histograms depict the number of filaments of each type (I, O, U or transitional) as a function of shock strength. Since half of the shocks are successful, the number of filaments in these cases is zero at 300 ms in all three major parts of the ventricles; it is also already zero at 100 ms at some locations in the ventricles. The weakest shock strength does not produce filaments in the LV.

Several interesting observations can be made from Fig. 11. The figure demonstrates that the number of filaments in transition between the three major filament types is very large early after the shock, as seen in the histograms at time point $t = 30$ ms. This transition can be responsible for the rapid decline in total number of filaments in the early stages after the shock, as presented in Fig. 9. The number of transitional filaments later decreases; however, transitions between the various types continue to take place as the activity evolves.

The majority of type O filaments (vortex rings), the most unstable filaments, are formed early after the shock. In Fig. 11, their number is the largest at $t = 30$ ms. Early septal activity appears dominated by vortex rings (in addition to transitional types). The initial number of O filaments (see $t = 30$ ms) is also the smallest in the RV. While some vortex rings are found in the later stages of ventricular activity, they seem to appear only in the

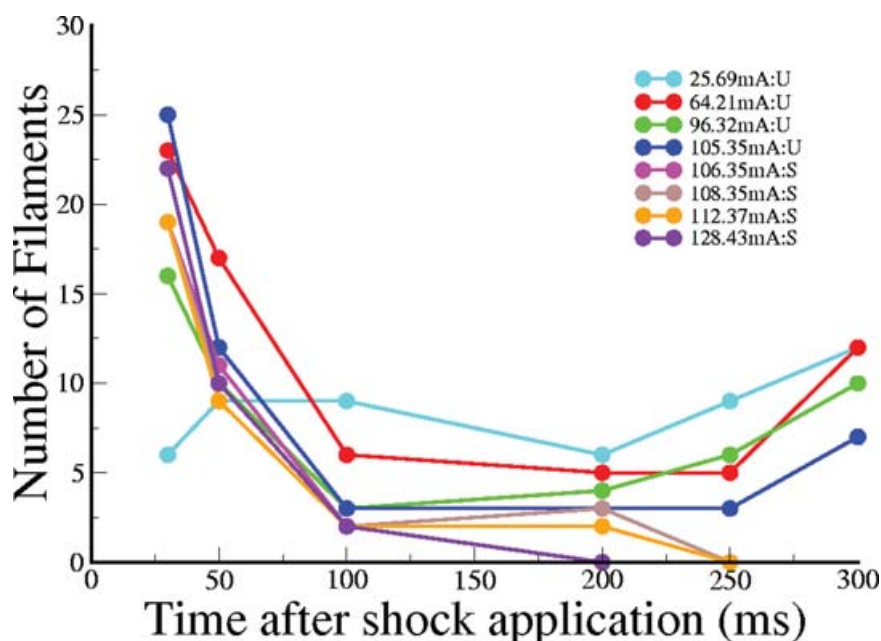


Figure 10. Plot of the number of post-shock filaments as a function of time after shock application for all 8 defibrillation shocks

Reproduced with permission from Trayanova *et al.* (2004). The shock strengths and colour key are shown in the inset. S, successful shock; U, unsuccessful shock.

LV and the septum, which are the thicker walls. One further observes that early after the end of the shock, type I filaments are found only in the RV (see histograms at $t = 30$ ms). However, regardless of location, type I is the dominant filament type in the activity sustained for more than 200 ms following the shock; as the histograms at $t = 300$ ms indicate, every failed shock is characterized with the formation of type I filaments in the three major parts of the ventricles. Finally, type U filaments are the main filament type in the LV during the first 100 ms after the shock. They are also a major player in the early RV activity.

Figure 11 also reveals that for successful shocks, the post-shock filament activity in the time interval 100–200 ms (right before all filaments disappear) is located only in the LV; the majority of these filaments are type U. Thus, in the case of successful shocks, the activity in the septum and the RV is extinguished earlier, with re-entry lingering only in the LV before the final annihilation of the remaining filaments. In fact, most of these remaining LV filaments are located on the epicardial surface of the LV. For failed shocks, the histograms demonstrate that the activity during this time interval is characterized by a lower overall number of filaments. This is consistent with the (nearly) flat stretch of the curves shown in Fig. 10.

In conclusion, the presented simulations of defibrillation in the rabbit ventricular model reveal that the number of shock-induced scroll-wave filaments is the largest at the end of the shock and rapidly decreases in the first 100 ms following shock delivery. For all successful

shocks, the filaments disappear completely within 250 ms of post-shock activity. For all failed shocks, the number of filaments increases again after 200–250 ms of post-shock activity. One of the most significant findings in this paper is that, in the case of shock success, the activity is maintained only in the LV, while in the RV and the septum the filaments vanish earlier. Thus, for successful shocks, re-entry in fact takes place only in the LV, while transient ‘seeds’ of re-entry that do not develop into full-blown circuits appear at all three major parts of the ventricles. Finally, the results reveal that the transitions between the various types of filaments are most frequent at the early stages of post-shock activity. Type I is the dominant filament type of the activity sustained for more than 200 ms after the shock, particularly in the RV.

Limitations and future directions

While the presented studies demonstrate an excellent match between simulation and experiment in terms of the pattern of VEP and shock-induced propagation, there remains a discrepancy between the values of simulated and measured VEP. The reason for this is that the optically recorded signal is distorted by photon scattering in the myocardium. In order to achieve a match between simulation and experiment in terms of shock-induced transmembrane potential values, the formation of optical signals based on transmembrane potential maps in the rabbit ventricles needs to be modelled. We have recently developed the first stage of such a model, and it is our hope

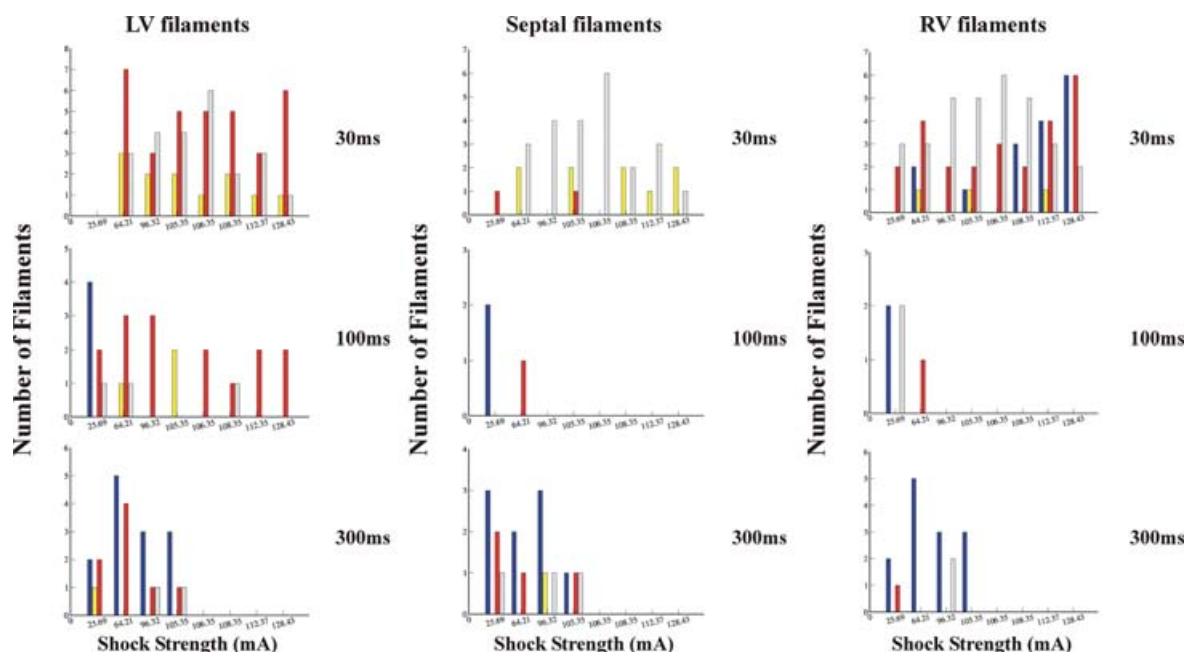


Figure 11. Number and type of filaments (I, U, O or transitional) as a function of shock strength for three post-shock timings, 30, 100 and 300 ms, in the left and right ventricular free walls and in the septum I filaments are shown in blue, O filaments are shown in yellow, U filaments are in red, and transitional filaments are shown in grey. Reproduced with permission from Trayanova *et al.* (2004).

that with the use of this model we can achieve in the future a more meaningful comparison between simulation results and experimental data. An important further step in this direction is to obtain a rabbit ventricular cell model that is based on experimental data for the membrane response to strong shocks, rather than relying on *ad hoc* adjustments of ionic models to represent defibrillation.

The 3-D model of defibrillation in the rabbit ventricles presented here is homogeneous, i.e. it does not incorporate microscale heterogeneities present in the myocardium; these might have significant effects on VEP, particularly under the conditions of fibrosis. Furthermore, the defibrillation mechanisms presented here might be altered in the diseased heart, where ischaemia and infarction are bound to modify the substrate for arrhythmigenesis following defibrillation shocks.

Concluding remarks

The two example studies included in this review article, one on vulnerability to electric shocks and one on defibrillation, clearly demonstrate the power of realistic modelling in revealing electrical behaviour hidden within the cardiac wall. When matched to experimental observations of behaviour during and after the shock over the cardiac surfaces, realistic whole-organ simulations become invaluable in elucidating the mechanisms of ventricular defibrillation. Insights into vulnerability and defibrillation such as those presented here are unachievable with experimental methodology alone owing to its present lack of ability to provide, with sufficient resolution, information about the 3-D electrical activity in the heart following defibrillation shocks.

References

- Aguel F, Eason J & Trayanova N (2003). Advances in modeling cardiac defibrillation. *Int J Bifurcation Chaos* **13**, 3791–3805.
- Al Khadra AS, Nikoloski V & Efimov IR (2000). The role of electroporation in defibrillation. *Circ Res* **87**, 797–804.
- Anderson C & Trayanova NA (2001). Success and failure of biphasic shocks: results of bidomain simulations. *Math Biosci* **174**, 91–109.
- Anderson C, Trayanova N & Skouibine K (2000). Termination of spiral waves with biphasic shocks: the role of virtual electrode polarisation. *J Cardiovasc Electrophysiol* **11**, 1386–1396.
- Ashihara T, Namba T, Ito M, Ikeda T, Nakazawa K & Trayanova N (2004). Spiral wave control by a localized stimulus: a bidomain model study. *J Cardiovasc Electrophysiol* **15**, 226–233.
- Ashihara T & Trayanova NA (2004). Asymmetry in membrane responses to electrical shocks: insight from bidomain simulations. *Biophys J* **87**, 2271–2282.
- Beeler GW & Reuter H (1977). Reconstruction of the action potential of ventricular myocardial fibres. *J Physiol* **268**, 177–210.
- Byars JL, Smith WM, Ideker RE & Fast VG (2003). Development of an optrode for intramural multisite optical recordings of V_m in the heart. *J Cardiovasc Electrophysiol* **14**, 1196–1202.
- Cheek ER & Fast VG (2004). Nonlinear changes of transmembrane potential during electrical shocks: role of membrane electroporation. *Circ Res* **94**, 208–214.
- Cheek ER, Ideker RE & Fast VG (2000). Nonlinear changes of transmembrane potential during defibrillation shocks: role of Ca^{2+} current. *Circ Res* **87**, 453–459.
- Chen PS, Shibata N, Dixon EG, Martin RO & Ideker RE (1986). Comparison of the defibrillation threshold and the upper limit of ventricular vulnerability. *Circulation* **73**, 1022–1028.
- Cheng DKL, Tung L & Sobie EA (1999a). Nonuniform responses of transmembrane potential during electric field stimulation of single cardiac cells. *Am J Physiol* **277**, H351–H362.
- Cheng Y, Mowrey KA, Van Wagoner DR, Tchou PJ & Efimov IR (1999b). Virtual electrode-induced reexcitation: a mechanism of defibrillation. *Circ Res* **85**, 1056–1066.
- Eason JC & Trayanova N (2002). Phase singularities and termination of spiral wave reentry. *J Cardiovasc Electrophysiol* **13**, 672–679.
- Efimov IR, Aguel F, Cheng Y, Wollenzier B & Trayanova N (2000a). Virtual electrode polarisation in the far field: implications for external defibrillation. *Am J Physiol Heart Circ Physiol* **279**, H1055–H1070.
- Efimov IR, Cheng Y, Van Wagoner DR, Mazgalev TN & Tchou PJ (1998). Virtual electrode induced phase singularity: a basic mechanism of defibrillation failure. *Circ Res* **82**, 918–925.
- Efimov IR, Cheng Y, Yamanouchi Y & Tchou PJ (2000b). Direct evidence of the role of virtual electrode induced phase singularity in success and failure of defibrillation. *J Cardiovasc Electrophysiol* **11**, 861–868.
- Efimov IR, Gray RA & Roth BJ (2000c). Virtual electrodes and deexcitation: new insights into fibrillation induction and defibrillation. *J Cardiovasc Electrophysiol* **11**, 339–353.
- Entcheva E, Trayanova NA & Claydon FJ (1999). Patterns of and mechanisms for shock-induced polarisation in the heart: a bidomain analysis. *IEEE Trans Biomed Eng* **46**, 260–270.
- Evans FG, Ideker RE & Gray RA (2002). Effect of shock-induced changes in transmembrane potential on reentrant waves and outcome during cardioversion of isolated rabbit hearts. *J Cardiovasc Electrophysiol* **13**, 1118–1127.
- Faber GM & Rudy Y (2000). Action potential and contractility changes in $[Na^+]_i$ overloaded cardiac myocytes: a simulation study. *Biophys J* **78**, 2392–2404.
- Fabiato A, Coumel P, Gourgon R & Saumont R (1967). Le seuil de reponse synchrone des fibres myocardiques. Application la comparaison experimentale de l'efficacit des diffrentes formes de chocs lectriques de difbrillation. *Arch Mal Cur* **60**, 527–544.
- Fast VG, Rohr S & Ideker RE (2000). Nonlinear changes of transmembrane potential caused by defibrillation shocks in strands of cultured myocytes. *Am J Physiol Heart Circ Physiol* **278**, H688–H697.
- Gray RA, Pertsov AM & Jalife J (1998). Spatial and temporal organization during cardiac fibrillation. *Nature* **392**, 675–678.

- Hillebrenner MG, Eason JC & Trayanova NA (2004). Mechanistic inquiry into the decrease in probability of defibrillation success with increase in complexity of preshock reentrant activity. *Am J Physiol Heart Circ Physiol* **286**, H909–H917.
- Hillebrenner MG, Eason JC, Campbell CA & Trayanova NA (2003). Postshock arrhythmogenesis in a slice of the canine heart. *J Cardiovasc Electrophysiol* **14**, S249–S256.
- Hodgkin AL & Rushton WAH (1946). The electrical constants of the crustacean nerve fibre. *Proc Royal Soc London* **133**, 444–479.
- Hooks DA, LeGrice IJ, Harvey JD & Smaill BH (2001). Intramural multisite recording of transmembrane potential in the heart. *Biophys J* **81**, 2671–2680.
- Hooks DA, Tomlinson KA, Marsden SG, LeGrice IJ, Smaill BH, Pullan AJ & Hunter PJ (2002). Cardiac microstructure: implications for electrical propagation and defibrillation in the heart. *Circ Res* **91**, 331–338.
- Knisley SB, Hill BC & Ideker RE (1994). Virtual electrode effects in myocardial fibres. *Biophys J* **66**, 719–728.
- Knisley SB, Trayanova N & Aguel F (1999). Roles of electric field and fibre structure in cardiac electric stimulation. *Biophys J* **77**, 1404–1417.
- Kwaku KF & Dillon SM (1996). Shock-induced depolarization of refractory myocardium prevents wave-front propagation in defibrillation. *Circ Res* **79**, 957–973.
- Larson C, Dragnev L & Trayanova N (2003). Analysis of electrically induced reentrant circuits in a sheet of myocardium. *Ann Biomed Eng* **31**, 768–780.
- Lindblom AE, Aguel F & Trayanova N (2001). Virtual electrode polarisation leads to reentry in the far field. *J Cardiovasc Electrophysiol* **12**, 946–956.
- Lindblom AE, Roth BJ & Trayanova N (2000). Role of virtual electrodes in arrhythmogenesis: pinwheel experiment revisited. *J Cardiovasc Electrophysiol* **11**, 274–285.
- Luo CH & Rudy Y (1991). A model of the ventricular cardiac action potential: depolarisation, repolarisation, and their interaction. *Circ Res* **68**, 1501–1526.
- Luo CH & Rudy Y (1994). A dynamic model of the ventricular cardiac action potential. I. Simulations of ionic currents and concentration changes. *Circ Res* **74**, 1071–1096.
- Rodriguez B, Li L, Eason JC, Efimov IR & Trayanova N (2005). Differences between left and right ventricular chamber geometry affect cardiac vulnerability to electric shocks. *Circ Res* **97**, 168–175.
- Rodriguez B, Tice BM, Eason JC, Aguel F, Ferrero JM Jr & Trayanova N (2004a). Effect of acute global ischemia on the upper limit of vulnerability: a simulation study. *Am J Physiol Heart Circ Physiol* **286**, H2078–H2088.
- Rodriguez B, Tice B, Eason J, Aguel F & Trayanova N (2004b). Cardiac vulnerability to electric shocks during phase 1a of acute global ischaemia. *Heart Rhythm* **6**, 695–703.
- Rodriguez B & Trayanova N (2003). Upper limit of vulnerability in a defibrillation model of the rabbit ventricles. *J Electrocardiol* **36** (Suppl.), 51–56.
- Roth BJ (1995). A mathematical model of make and break electrical stimulation of cardiac tissue by a unipolar anode or cathode. *IEEE Trans Biomed Eng* **42**, 1174–1184.
- Sepulveda NG, Roth BJ & Wikswo JP Jr (1989). Current injection into a two-dimensional anisotropic bidomain. *Biophys J* **55**, 987–999.
- Skouibine K, Trayanova N & Moore PK (1999). Anode/cathode make and break phenomena in a model of defibrillation. *IEEE Trans Biomed Eng* **46**, 769–777.
- Skouibine K, Trayanova N & Moore P (2000a). Success and failure of the defibrillation shock: insights from a simulation study. *J Cardiovasc Electrophysiol* **11**, 785–796.
- Skouibine K, Trayanova N & Moore PK (2000b). A numerically efficient model for simulation of defibrillation in an active bidomain sheet of myocardium. *Math Biosci* **166**, 85–100.
- Sobie EA, Susil RC & Tung L (1997). A generalized activating function for predicting virtual electrodes in cardiac tissue. *Biophys J* **73**, 1410–1423.
- Trayanova N (1999). Far field stimulation of cardiac tissue. *Herzschrittmacher Therapie Electrophysiologie* **10**, 137–148.
- Trayanova N (2001). Concepts of ventricular defibrillation. *Phil Trans R Soc Lon A* **359**, 1327–1337.
- Trayanova N, Aguel F, Larson C & Haro C (2004). Modeling cardiac defibrillation: an inquiry into post shock dynamics. In *Cardiac Electrophysiology: from Cell to Bedside*, 4th edn, ed. Zipes D & Jalife J, pp. 282–291. W. B. Saunders Co, Philadelphia.
- Trayanova N, Aguel F & Skouibine K (1999). Extension of refractoriness in a model of cardiac defibrillation. In *Proceedings of the Pacific Symposium on Biocomputing*, ed. Altman RB, Dunker AK, Hunter L, Klein TE & Lauderdale K, pp. 240–251. World Scientific, Singapore.
- Trayanova N & Bray MA (1997). Membrane refractoriness and excitation induced in cardiac fibres by monophasic and biphasic shocks. *J Cardiovasc Electrophysiol* **8**, 745–757.
- Trayanova N & Eason J (2002). Shock-induced arrhythmogenesis in the myocardium. *Chaos* **359**, 1327–1337.
- Trayanova N, Eason JC & Aguel F (2002a). Computer simulations of cardiac defibrillation: a look inside the heart. *Comput Visualiz Sci* **4**, 259–270.
- Trayanova N, Eason JC, Anderson C & Aguel F (2002b). Computer modeling of defibrillation II: Why does the shock fail? In *Quantitative Cardiac Electrophysiology*, ed. Cabo C & Rosenbaum D, pp. 235–256. Marcel Dekker, New York.
- Trayanova N, Gray R, Bourn D & Eason JC (2003). Virtual electrode-induced positive and negative graded responses: new insights into fibrillation induction and defibrillation. *J Cardiovasc Electrophysiol* **14**, 756–763.
- Trayanova N & Skouibine K (1998). Modeling defibrillation: effects of fibre curvature. *J Electrocardiol* **31** (Suppl.), 23–29.
- Trayanova N, Skouibine K & Aguel F (1998a). The role of cardiac tissue structure in defibrillation. *Chaos* **8**, 221–233.
- Trayanova N, Skouibine K & Moore PK (1998b). Virtual electrode effects in defibrillation. *Prog Biophys Mol Biol* **69**, 387–403.
- Vetter FJ & McCulloch AD (1998). Three-dimensional analysis of regional cardiac function: a model of rabbit ventricular anatomy. *Prog Biophys Mol Biol* **69**, 157–183.
- Wiggers CJ (1930). Studies of ventricular fibrillation caused by electric shock: cinematographic and electrocardiographic observations of the natural process in the dog's heart: its inhibition by potassium and the revival of coordinated beats by calcium. *Am J Physiol* **5**, 351–365.

- Wikswow JP Jr, Lin SF & Abbas RA (1995). Virtual electrodes in cardiac tissue: a common mechanism for anodal and cathodal stimulation. *Biophys J* **69**, 2195–2210.
- Winfrey A (1987). *When Time Breaks Down*. Princeton University Press, Princeton, NJ, USA.
- Winfrey AT (1988). Varieties of spiral wave behavior: an experimentalist's approach to the theory of excitable media. *Chaos* **1**, 303–334.

Zhou X, Rollins DL, Smith WM & Ideker RE (1995). Responses of the transmembrane potential of myocardial cells during a shock. *J Cardiovasc Electrophysiol* **6**, 252–263.

Acknowledgements

This work was supported by National Institutes of Health grants HL063195, HL074283 and HL067322, and a grant from the American Heart Association.

Defibrillation of the heart: insights into mechanisms from modelling studies
Natalia Trayanova

Exp Physiol 2006;91;323-337; originally published online Feb 9, 2006;

DOI: 10.1113/expphysiol.2005.030973

This information is current as of December 18, 2007

Updated Information & Services	including high-resolution figures, can be found at: http://ep.physoc.org/cgi/content/full/91/2/323
Subspecialty Collections	This article, along with others on similar topics, appears in the following collection(s): Heart/Cardiac Muscle http://ep.physoc.org/cgi/collection/heart_cardiac_muscle
Permissions & Licensing	Information about reproducing this article in parts (figures, tables) or in its entirety can be found online at: http://ep.physoc.org/misc/Permissions.shtml
Reprints	Information about ordering reprints can be found online: http://ep.physoc.org/misc/reprints.shtml